Recently, Nederberg et al. reported on the synthesis and characterization of phosphorylcholine-end capped poly(ε-caprolactone) (PCL-PC) as polymeric additives in a poly(ε-caprolactone) (PCL) membrane. Surface rearrangement and enrichment of the PCL-PC occurred on the PCL membrane by use of the hot-water treatment and resulted in improved surface wettability.[21,22] An environmentally responsive surface (smart surface) with a polymer blend was also demonstrated by Anastasiadis et al.[23] They synthesized polystyrene-*block*-polyisoprene diblocks with hydrophilic groups such as a sulfobetaine- and a dimethylamine group at the end of a low energy polyisoprene block and mixed with polystyrene homopolymer.[23] The wettability of the blend polymer changed with environmental humidity. The surface response demonstrated good harmonization of a hydrophilic functional group and the polyisoprene block. To make additives having PC groups and low energy chemicals or polymers, spontaneous PC-enriched surfaces would be obtained from polymer blending.

We report here on the preparation of highly wettable polyethylene films with small amounts of perfluoroalkylated phosphorylcholine (PC) additives by the heat-press technique. The effects of chemical structure and fluoroalkyl chain length on surface modification were studied.

EXPERIMENTAL

Materials

2-(Perfluorohexyl)ethanol ($C_6F_{13}OH$), 2-(perfluorooctyl)ethanol ($C_8F_{17}OH$), and 2-(perfluorodecyl)ethanol ($C_{10}F_{21}OH$) were purchased from Daikin, Tokyo, Japan. 2-Chloro-2-oxo-1,3,2-dioxaphospholane (COP) was obtained from NOF, Tokyo, Japan. Tetrahydrofuran (THF), acetonitrile (MeCN), triethylamine (TEA), and trimethylamine (TMA) were purified by distillation. All other chemicals were used without further purification.

Synthesis of perfluoroalkylated phosphorylcholines ($C_nF_{2n+1}PCs$)

Perfluoroalkylated phosphorylcholines (n = 6, 8, 10) were synthesized by an improved process of MPC synthesis.[24] Briefly, a solution of 6.43 g (45.0 mmol) of 2-chloro-2-oxo-1,3,2-dioxaphospholane in 25 mL of dry THF was added dropwise to a mixture of 16.38 g (45.0 mmol) of $C_6F_{13}OH$ and 4.55 g (45.mmol) of TEA in 120 mL dry THF at 0°C for 1 h and at room temperature for another 1 h under a nitrogen atmosphere. The triethylamine hydrochloride salt precipitate was filtered off. The filtrate was evaporated under reduced pressure up to half its volume. The concentrated solution of 1-(2-oxo-1,3,2-dioxaphospholan-2-yloxy)-2-(perfluorohexyl)ethane and 150 mL of dry MeCN were placed in a glass pressure bottle. After the mixture was cooled to −20°C, 15 mL of anhydrous TMA was added, and the reaction was allowed to continue at 70°C for 12 h. The reaction mixture was again cooled to −20°C to precipitate 2-(perfluorohexyl)ethyl phosphorylcholine ($C_6F_{13}PC$).

^{1}H NMR (CD_3OD) δ = 2.59 (m, CF_2CH_2, 2H), 3.21 (s, $-N^+(CH_3)_3$, 9H), 3.63 (t, $-CH_2N^+$, 2H), 4.19 (m, $-CH_2OP-$, 2H), 4.27(br, $-OPCH_2-$, 2H); ^{19}F NMR (CD_3OD) δ = −81.40 (CF_3, 3F), −113.39 (CF_2CH_2, 2F), −121.75 ($(CF_2)_3CF_2CH_2$, 6H), −122.58 ($CF_3CF_2CF_2CF_2CF_2$, 2F), −123.49 ($CF_3CF_2CF_2$, 2F), −126.11 (CF_3CF_2, 2F); IR (cm^{-1}): 2910 (—CH_2—), 1300 (P=O), 1235 (—OPO—), 1085 (—$OPOCH_2$—), 970 ($N^+(CH_3)_3$).

$C_8F_{17}PC$ and $C_{10}F_{21}PC$ were also synthesized by a method similar to that described above. Hexadecyl phosphorylcholine ($C_{16}PC$) was synthesized as previously reported.[25] Figure 1 shows the chemical structure of the PC additives synthesized in this study.

Preparation of composite low-density polyethylene films with PC additives

The low-density polyethylene (LDPE) used as the base material in particle form was purchased from Sumitomo Seika Chemicals (Flow beads LE-1080, Osaka, Japan). The average diameter was 6 μm.

The LDPE and composite films with PC additives were processed by a heat-press technique. Typically, the LDPE particles (0.5 g) and 2-(perfluorodecyl)ethyl phosphorylcholine ($C_{10}F_{21}PC$, 0.05 g, 6.86×10^{-5} mol) were mixed and thoroughly ground in a mortar. The mixed powder was then placed between two stainless steel plates and pressed at a pressure of about 5 MPa at 120°C for 3 min. To determine the appropriate $C_{10}F_{21}PC$ composition, we prepared films with different blend ratios [$C_{10}F_{21}PC$/LDPE = 1/10 (0.05 g, 6.86×10^{-5} mol/0.5 g); 1/25 (0.02 g, 2.74×10^{-5} mol/0.5 g); 1/50 (0.01 g, 1.37×10^{-5} mol/0.5 g); and 1/100 (0.005 g, 6.86×10^{-6} mol/0.5 g) by weight]. Other PC compounds were mixed with LDPE particles with molar compositions similar to that of $C_{10}F_{21}PC$.

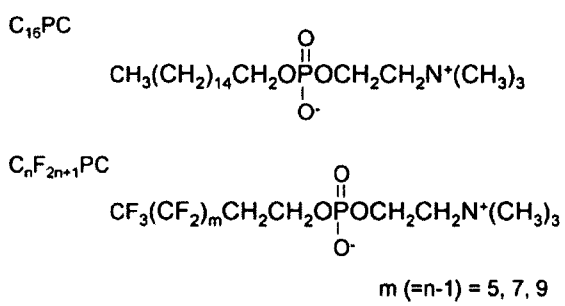

Figure 1 Chemical structure of alkylated and perfluoroalkylated PC.

To determine the elution amount of the PC additives from the composite films, the films were immersed in water or ethanol with gentle shaking. The solvents were changed three times at 2-h intervals, and the concentration of the PC additives was determined by phosphorus analysis.

Surface analysis

X-ray photoelectron spectroscopy (XPS) was performed on a Scienta ESCA-200 spectrometer with Al Kα. Survey scan spectra of C_{1s}, O_{1s}, N_{1s}, P_{2p}, and F_{1s} were obtained. All XPS data were collected at takeoff angles of 15° and 75° (between the specimen surface and the detector).

The dynamic contact angles for the samples were recorded as the probe fluid, water (deionized to 18.2 MΩ), using a First Ten Angstroms FT-125 goniometer and Gilmont syringes. The advancing (θ_A) and receding (θ_R) contact angles were measured at addition to and withdrawal from the drop, respectively.

Evaluation of mechanical properties

Tensile strength measurements were performed using an STA-1150 (ORIENTEC, Tokyo, Japan). The samples were cut into dog-bone shape (size, 12.5 mm × 2.5 mm). The crosshead speed was 2 mm/min. Four specimens were tested. Within the region of elongation from 0 to 5%, the strain–stress curves were linear. Young's modulus was then obtained from this initial elastic region.

RESULTS AND DISCUSSION

Surface activity of perfluoroalkylated PCs

The perfluoroalkylated PCs with different perfluoroalkyl chain lengths were obtained as a white powder. C_6F_{13}PC was readily soluble in water and ethanol. C_8F_{17}PC and C_{16}PC were soluble in water, but the solutions at this concentration were very viscous, resembling hydrogel, indicating that the intramolecular interaction of these molecules is high in an aqueous solution. In addition, the C_{16}PC aqueous solution was turbid. These additives were easily soluble in ethanol. In contrast, $C_{10}F_{21}$PC was not soluble in water or ethanol.

Several groups have shown that perfluoroalkyl groups that are incorporated into polymers are surface active[7,26–33] and adsorb at free polymer interfaces due to minimization of surface free energy. We tested the incorporation of the perfluoroalkyl groups with the PC groups to enhance the efficiency of the

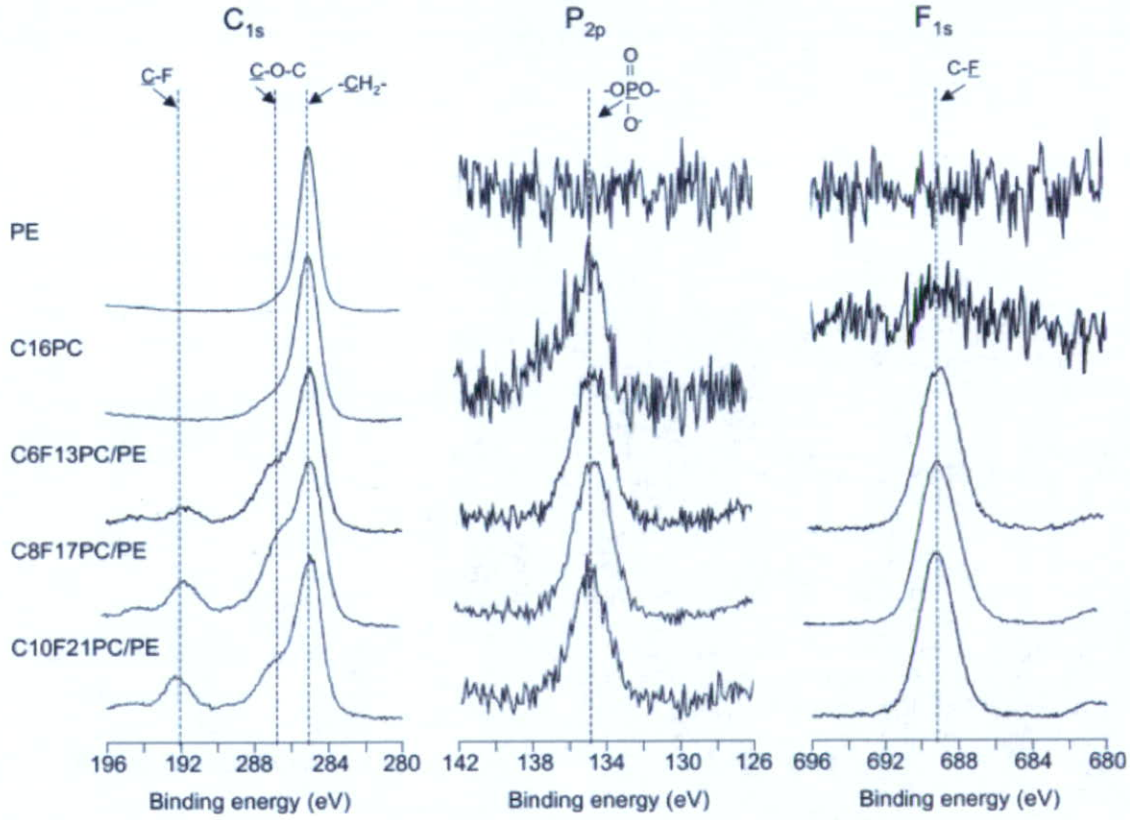

Figure 2 XPS spectra of PE and composite polymer films.

TABLE I
XPS Data for Polymer Films

Films	Composition of PC additives (mol)	Composition of PC additives (% w/w)	Takeoff angle (°)	XPS elemental data (%) C	O	N	P	F
$C_{16}PC/PE$	6.86×10^{-6}	0.6	15	90.07	8.96	0.34	0.63	
			75	98.71	1.07	0.19	0.03	
	1.37×10^{-5}	1.1	15	94.21	4.43	0.45	0.91	
			75	96.54	2.65	0.45	0.36	
	2.74×10^{-5}	2.2	15	88.74	8.84	1.18	1.24	
			75	91.40	6.71	0.82	1.07	
	6.86×10^{-5}	5.3	15	93.75	3.20	1.50	1.55	
$C_{10}F_{21}/PC/PE$	6.86×10^{-6}	1.0	15	84.45	7.06	0.64	0.58	7.27
			75	80.73	4.97	0.33	0.54	13.43
	1.37×10^{-5}	2.0	15	76.17	7.03	0.42	0.93	15.45
			75	82.93	4.07	0.33	0.43	12.24
	2.74×10^{-5}	3.8	15	56.30	9.17	0.67	1.48	32.38
			75	42.49	10.33	1.19	1.95	44.04
	6.86×10^{-5}	9.1	15	65.10	7.20	2.40	2.30	23.00
$C_8F_{17}/PC/PE$	6.86×10^{-6}	0.9	15	84.51	7.30	0.37	1.18	6.64
			75	89.04	2.87	0.23	0.36	7.50
	1.37×10^{-5}	1.7	15	36.37	6.71	1.07	2.62	53.23
			75	47.67	10.04	1.20	1.73	39.36
	2.74×10^{-5}	3.3	15	38.26	8.02	1.76	2.64	49.32
			75	48.32	10.62	1.07	1.94	38.05
	6.86×10^{-5}	7.9	15	37.50	8.00	2.00	2.80	49.70
$C_6F_{15}/PC/PE$	6.86×10^{-6}	0.7	15	80.77	8.89	0.47	1.08	8.79
			75	75.34	7.38	0.68	0.81	15.79
	1.37×10^{-5}	1.4	15	79.32	3.88	0.49	1.36	14.95
			75	85.63	3.14	0.46	0.57	10.20
	2.74×10^{-5}	2.8	15	58.17	13.27	1.25	1.80	25.51
			75	60.98	11.03	1.14	1.80	25.05
	6.86×10^{-5}	6.8	15	52.90	10.90	2.50	2.10	31.60

additives in the LDPE films that resulted in highly hydrophilic surfaces.

Figure 2 shows the XPS spectra of LDPE and composite films, which are corrected at a takeoff angle of 15°. For the original LDPE film, a strong intensity at 285 eV was observed and attributed to carbon atoms in the methylene chains of the polyethylene backbone. Mixing the PC additives with the PE particles dramatically changed the XPS spectra of the fabricated films. In every C_{1s} spectrum of the composite films, a shoulder was observed at 286.5 eV. This shoulder could be attributed to the ether bonds (C—O) of the PC additives. In addition, for films mixed with fluoroalkylated PCs a peak was observed at 290 eV. This peak corresponded to the carbon atom bonded to fluorine (C—F). A peak ascribed to phosphorus was observed at 134.1 eV. This could be attributed to the phosphorylcholine group in the PC additives. The spectra of the phosphorus of the films containing fluoroalkylated PCs were clearer than that of those containing $C_{16}PC$. This means that enrichment of fluoroalkylated PC is preferred. At 680 eV, a fluorine signal was also observed on the fluoroalkylated PC composite film.

The XPS elemental concentrations for the polymer films are summarized in Table I. The nitrogen and phosphorus concentrations increased with an increase in the composition of the PC additives in the feed. In particular, the surface concentrations for these elements were remarkably high when $C_8F_{17}PC$ was used as the additive. Figure 3 shows the effect of the PC additives on surface enrichment of the composite films. While the P/C ratio did not change remarkably with the bulk composition of $C_{16}PC$, the ratio did increase with an increase in the composition of perfluoroalkylated phos-

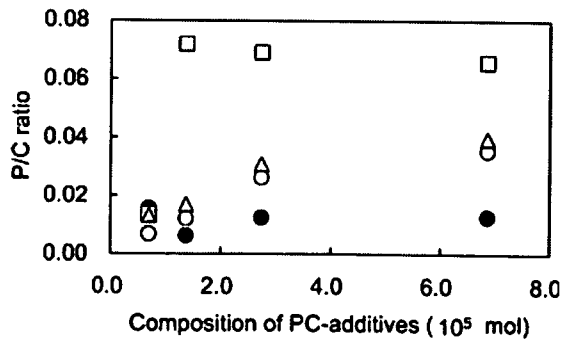

Figure 3 Surface P/C ratio versus bulk composition films. Filled circle: $C_{16}PC/PE$, Open circle: $C_6F_{13}PC/PE$, Open square: $C_8F_{17}PC/PE$, Open triangle: $C_{10}F_{21}PC/PE$.

phorylcholine. In particular, the phosphorus concentration of the $C_8F_{17}PC$/LDPE film was significantly higher than that of other composite films with low molar $C_8F_{17}PC$ (1.37×10^{-5} mol, 1.7% w/w).

The 15° takeoff angle data indicate the composition of the outermost ~ 10 Å of the samples; the 75° takeoff angle spectra assess the outer ~ 40 Å.[34] Comparison of the atomic concentration obtained from XPS to the chemical composition of $C_8F_{17}PC$ (C, 29.63%; O, 10.17%, N, 2.23; P, 4.92%; F, 51.33%) indicates that there is ~ 95% $C_8F_{17}PC$ in the outer 10 Å and ~ 75% $C_8F_{17}PC$ in the outer 40 Å when the compositions are calculated from the concentration of fluorine. From the concentration of phosphorus, there is ~ 55% $C_8F_{17}PC$ in the outer 10 Å and ~ 40% $C_8F_{17}PC$ in the outer 40 Å. The molecular size of $C_8F_{17}PC$ is ~ 18 Å, and the fluoroalkyl chains of $C_8F_{17}PC$ were partially oriented to the outer surface. When $C_6F_{13}PC$ and $C_{10}F_{21}PC$ were added to LDPE with a similar concentration (2.74×10^{-5} mol), the surface coverage calculated from the concentration of fluorine was ~ 55% and ~ 60% in the outer 10 Å, respectively. For $C_6F_{13}PC$, the surface coverage calculated from the concentration of phosphorus was 30%; the XPS elemental concentrations at 15° and 75° were quite similar. This result indicated that the distribution of $C_6F_{13}PC$ in the outer 40 Å was uniform. Moreover, the concentration of fluorine in the outer 40 Å was higher than that in the outer 10 Å when $C_{10}F_{21}PC$ (2.74×10^{-5} mol) was added. The surface activity and dispersity of $C_8F_{17}PC$ in the LDPE matrix may be optimum for the enrichment of LDPE film surfaces.

Surface contact angle data for polymer films were measured with water, as shown in Table II. The water contact angle data for the LDPE film was $\theta_A/\theta_R = 97°/81°$. The contact angles decreased with an increase in the composition of the PC additives. On the $C_{16}PC$/LDPE surface, the contact angles reached $\theta_A/\theta_R = 43°/15°$ when the composition of $C_{16}PC$ was 6.86×10^{-5} mol (5.3% w/w). At this concentration, the surface coverage of $C_{16}PC$ was ~ 15% calculated from XPS data and was lower than that of fluoroalkylated PCs. The water contact angles of the $C_{16}PC$/LDPE film were then relatively high.

The surface contact angles (θ_A/θ_R) of $C_8F_{17}PC$/LDPE were dramatically decreased at 28°/8° with 2.74×10^{-5} mol $C_8F_{17}PC$ (3.3% w/w) and 17°/< 5° with 6.86×10^{-5} mol $C_8F_{17}PC$ (7.9% w/w). The effects of $C_6F_{13}PC$ and $C_{10}F_{21}PC$ on improving surface wettability were less than that of $C_8F_{17}PC$ because of their low surface coverage.

Figure 4 shows % elution of PC additives from composite films after soaking films containing 6.86×10^{-5} mol of PC additives in ethanol for 2 h. The elution amount of fluoroalkyl PCs was significantly lower than that of alkyl PCs. In particular, the elution amount of $C_8F_{17}PC$ and $C_{10}F_{21}PC$ was reduced with an increase in the soaking frequency and elution did not occur after three soakings. The elution amount of PC additives from LDPE films in water was also determined to be much lower than that in ethanol and $C_8F_{17}PC$ after 24 h of soaking under gentle shaking. The amount was 0.4% or less for 6.86×10^{-5} mol (7.9% w/w) and 0.1% or less for 1.37×10^{-5} mol

TABLE II
Water Contact Angle Data for Polymer Films

Films	Composition of PC additives (mol)	Composition of PC additives (% w/w)	θ_A/θ_R (°) Post-preparation	θ_A/θ_R (°) After soaking in EtOH
PE			98/81	105/92
$C_{16}PC$/PE	6.86×10^{-6}	0.6	87/61	
	1.37×10^{-5}	1.1	87/68	
	2.74×10^{-5}	2.2	64/30	75/17
	6.86×10^{-5}	5.3	43/15	41/17
$C_{10}F_{21}$/PC/PE	6.86×10^{-6}	1.0	86/65	
	1.37×10^{-5}	2.0	93/55	
	2.74×10^{-5}	3.8	90/59	81/26
	6.86×10^{-5}	9.1	38/10	91/21
C_8F_{17}/PC/PE	6.86×10^{-6}	0.9	82/67	
	1.37×10^{-5}	1.7	81/8	
	2.74×10^{-5}	3.3	28/8	16/10
	6.86×10^{-5}	7.9	17/<5	18/10
C_6F_{15}/PC/PE	6.86×10^{-6}	0.7	84/62	
	1.37×10^{-5}	1.4	79/29	
	2.74×10^{-5}	2.8	68/32	94/55
	6.86×10^{-5}	6.8	26/11	26/10

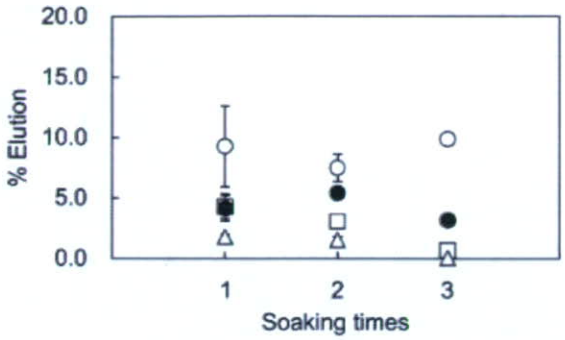

Figure 4 Percentage elution of PC additives from composite films soaked in ethanol. Filled circle: $C_{16}PC/PE$, Open circle: $C_6F_{13}PC/PE$, Open square: $C_8F_{17}PC/PE$, Open triangle: $C_{10}F_{21}PC/PE$.

(1.7% w/w). This solvent dependence of the elution might be due to the solubility of the PC additives.

Molecular design such as macromolecular approaches to improve stability and further surface treatments to reduce elution of PC additives from composite films are now under study.

Figure 5 shows photographs of typical water drops on LDPE and $C_8F_{17}PC/LDPE$ after the elution test in ethanol. When a water drop on LDPE film is round in shape, the shape spreads out completely on the $C_8F_{17}PC/PE$ film with 2.74×10^{-5} mol of $C_8F_{17}PC$ (3.3% w/w). The surface wettability of the composite film was present even after ethanol soaking, as shown in Table II.

Mechanical properties of LDPE films containing PC additives

Table III shows the mechanical properties of the composite films. By mixing PC additives, Young's modulus of films was relatively higher than that of the LDPE film. Every PC additive was a powdery solid at the measuring temperature and the composite films were then rigid. When the fracture strength was not changed by the addition of PC additives, the elongation of the composite films was reduced. This phenomenon might be due to an incompatibility of the PC additives and LDPE matrix. Although $C_{16}PC$ has a long alkyl chain, which would be more compatible with PE compared with that of the perfluoroalkylated chain, the elongation of the composite film with $C_{16}PC$ was much less. Fluoroalkylated PCs effectively enriched the LDPE surface and had less influence on the bulk property of the LDPE films.

CONCLUSIONS

Perfluoroalkylated PCs are potential additives for improving the wettability of LDPE film. Perfluoroalkylated PC was spontaneously enriched on the film surface using a heat-press technique. High wettability can be obtained without chemical or physical treatment. In addition, no solvent was needed. In particular, $C_8F_{17}PC$, which has an octafluoromethylene chain, is most effective for achieving this. The thermal stability of phosphorylcholine groups has been assured at 150°C.[35] Therefore, perfluoroalkylated PCs can be applied for surface modification of other thermoplastic polymers.

There has been a considerable amount of physicochemical- and biotechnological-related interest in PC-enriched surfaces, which show unique properties such as hydrophilicity,[36] zero ζ-potential (neutral),[37] high lubrication,[38] and biocompatibility.[39] Therefore, surface modification with spontaneous PC enrichment is important for producing high performance polymeric materials.

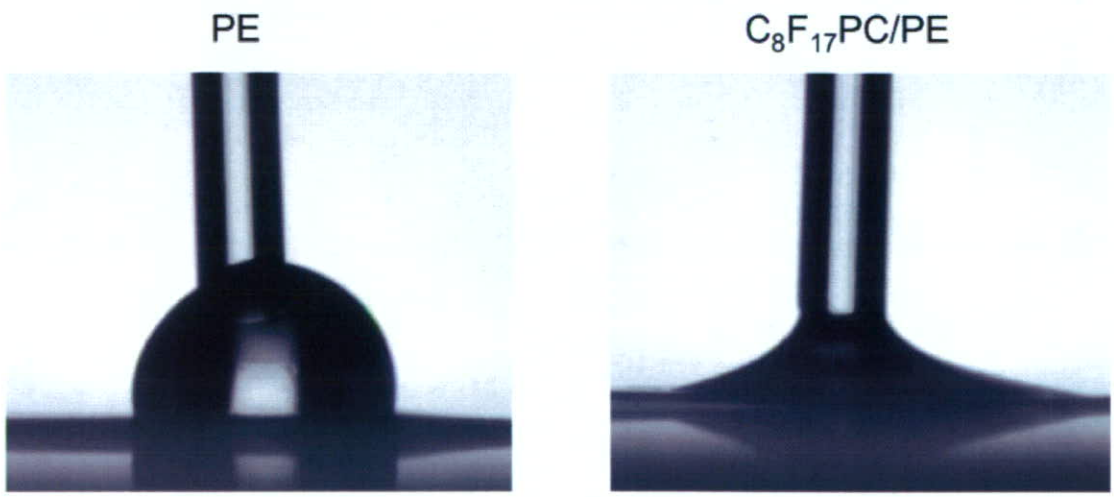

Figure 5 Photographs of water drops on PE and $C_8F_{17}PC/PE$ films ($C_8F_{17}PC = 1.37 \times 10^{-5}$ mol) after elution test.

TABLE III
Mechanical Properties of Polymer Films

	Composition of PC additives		Young's modulus (MPa)	Fracture strength (MPa)	Averaged fracture strain (%)
	(mol)	(% w/w)			
PE			61.9 ± 1.5	5.83 ± 0.32	80.1
C_{16}PC/PE	2.74	2.2	71.6 ± 4.4	5.49 ± 0.44	45.9
	6.86	5.3	60.8 ± 2.7	5.45 ± 0.32	46.3
$C_{10}F_{21}$/PC/PE	2.74	3.8	75.7 ± 5.3	5.72 ± 0.36	52.1
	6.86	9.1	68.3 ± 3.1	5.49 ± 0.25	58.3
C_8F_{17}/PC/PE	2.74	3.3	79.3 ± 6.9	6.00 ± 0.23	57.4
	6.86	7.9	68.9 ± 3.6	5.53 ± 0.19	56.5
C_6F_{15}/PC/PE	2.74	2.8	75.2 ± 1.1	5.68 ± 0.43	60.3
	6.86	6.8	68.5 ± 4.4	5.56 ± 0.28	54.1

The authors gratefully acknowledge the valuable support provided by Dr. Kazuhiko Ishihara of The University of Tokyo and Dr. Eui-Chul Kang of NOF Corporation. A part of this study was supported by NOF Corporation, Tokyo, Japan.

References

1. Andrade, J. D. Surface and Interfacial Aspects of Biomedical Polymers, Vol. 1: Surface Chemistry and Physics; Plenum: New York, 1985.
2. Ruardy, T. G.; Schakenraad, J. M.; vanderMei, H. C.; Busscher, H. J. Surf Sci Rep 1997, 29, 3.
3. Kano, Y.; Akiyama, S. Polymer 1996, 37, 4497.
4. Thomas, R. T.; Anton, D. R.; Graham, W. F.; Darmon, M. J.; Sauer, B. B.; Stika, K. M.; Swartzfager, D. G. Macromolecules 1997, 30, 2883.
5. Chen, W.; McCarthy, T. J. Macromolecules 1999, 32, 2342.
6. Ebbens, S. J.; Badyal, J. P. S. Langmuir 2001, 17, 4050.
7. Walters, K. B.; Schwark, D. W.; Hirt, D. E. Langmuir 2003, 19, 5851.
8. McCloskey, C. B.; Yip, C. M.; Santerre, J. P. Macromolecules 2002, 35, 924.
9. Yuan, Y.; Shoichet, M. S. Macromolecules 2000, 33, 4926.
10. Iwasaki, Y.; Mikami, A.; Kurita, K.; Yui, N.; Ishihara, K.; Nakabayashi, N. J Biomed Mater Res 1997, 36, 508.
11. Iwasaki, Y.; Sawada, S.; Nakabayashi, N.; Khang, G.; Lee, H. B.; Ishihara, K. Biomaterials 1999, 20, 2185.
12. Ishihara, K.; Ishikawa, E.; Iwasaki, Y.; Nakabayashi, N. J Biomater Sci Polym Ed 1999, 10, 1047.
13. Iwasaki, Y.; Nakabayashi, N.; Ishihara, K. J Biomed Mater Res 2001, 57, 72.
14. Ishihara, K.; Oshida, H.; Endo, Y.; Ueda, T.; Watanabe, A.; Nakabayashi, N. J Biomed Mater Res 1992, 26, 1543.
15. Ishihara, K.; Nomura, H.; Mihara, T.; Kurita, K.; Iwasaki, Y.; Nakabayashi, N. J Biomed Mater Res 1998, 39, 323.
16. Iwasaki, Y.; Sawada, S.; Ishihara, K.; Khang, G.; Lee, H. B. Biomaterials 2002, 23, 3897.
17. Sawada, S.; Sakaki, S.; Iwasaki, Y.; Nakabayashi, N.; Ishihara, K. J Biomed Mater Res A 2003, 64, 411.
18. Ishihara, K.; Shibata, N.; Tanaka, S.; Iwasaki, Y.; Kurosaki, T.; Nakabayashi, N. J Biomed Mater Res 1996, 32, 401.
19. Hasegawa, T.; Iwasaki, Y.; Ishihara, K. Biomaterials 2001, 22, 243.
20. Ishihara, K.; Nishiuchi, D.; Watanabe, J.; Iwasaki, Y. Biomaterials 2004, 25, 1115.
21. Nederberg, F.; Bowden, T.; Nilsson, B.; Hong, J.; Hilborn, J. J Am Chem Soc 2004, 126, 15350.
22. Nederberg, F.; Bowden, T.; Hilborn, J. Macromolecules 2004, 37, 954.
23. Anastasiadis, S. H.; Retsos, H.; Pispas, S.; Hadjichristidis, N.; Neophytides, S. Macromolecules 1994, 2003, 36.
24. Ishihara, K.; Ueda, T.; Nakabayashi, N. Polym J 1990, 22, 355.
25. Kang, E. C.; Kataoka, S.; Kato, K. Bull Chem Soc Jpn 2005, 78, 1558.
26. Iyengar, D. R.; Perutz, S. M.; Dai, C.-A.; Ober, C. K.; Kramer, E. J. Macromolecules 1996, 29, 1229.
27. Schaub, T. F.; Kellogg, G. J.; Mayes, A. M.; Kulasekere, R.; Ankner, J. F.; Kaiser, H. Macromolecules 1996, 29, 3982.
28. Affrossman, S.; Bertrand, P.; Hartshorne, M.; Kiff, T.; Leonard, D.; Pethrick, R. A.; Richards, R. W. Macromolecules 1996, 29, 5432.
29. Affrossman, S.; Hartshorne, M.; Kiff, T.; Pethrick, R. A.; Richards, R. W. Macromolecules 1994, 27, 1588.
30. Elman, J. F.; Johs, B. D.; Long, T. E.; Koberstein, J. T. Macromolecules 1994, 27, 5341.
31. Hunt, M. O., Jr.; Belu, A. M.; Linton, R. W.; DeSimone, J. M. Macromolecules 1993, 26, 4854.
32. Su, Z.; Wu, D.; Hsu, S. L.; McCarthy, T. J. Macromolecules 1997, 30, 840.
33. Chen, W.; Franchina, N. L.; Viviano, K.; McCarthy, T. J. Polym Mater Sci Eng 1996, 75, 44.
34. Clark, D. T.; Thomas, H. R. J Polym Sci Polym Chem Ed 1977, 15, 2843.
35. Ogawa, R.; Iwasaki, Y.; Ishihara, K. J Biomed Mater Res 2003, 62, 214.
36. Iwata, R.; Suk-In, P.; Hoven, V. P.; Takahara, A.; Akiyoshi, K.; Iwasaki, Y. Biomacromolecules 2004, 5, 2308.
37. Ishihara, K.; Inoue, H.; Kurita, K.; Nakabayashi, N. J Biomed Mater Res 1994, 28, 1347.
38. Moro, T.; Takatori, Y.; Ishihara, K.; Konno, T.; Takigawa, Y.; Matsushita, T.; Chung, U. I.; Nakamura, K.; Kawaguchi, H. Nat Mater 2004, 3, 829.
39. Iwasaki, Y.; Ishihara, K.; 2005, Anal Bioanal Chem 2005, 381, 534.

Available online at www.sciencedirect.com
SCIENCE DIRECT
Materials Research Bulletin 41 (2006) 515–524
Materials Research Bulletin
www.elsevier.com/locate/matresbu

Enhancement of mechanical strength of TiO_2/high-density polyethylene composites for bone repair with silane-coupling treatment

Masami Hashimoto [a,*], Hiroaki Takadama [a], Mineo Mizuno [a], Tadashi Kokubo [b,1]

[a] *Japan Fine Ceramics Center, 2-4-1 Mutsuno, Atsuta-ku, Nagoya 456-8587, Japan*
[b] *Research Institute for Science and Technology, Chubu University, 1200 Matsumoto-cho, Kasugai 487-8501, Japan*

Received 14 April 2005; received in revised form 7 September 2005; accepted 19 September 2005
Available online 7 October 2005

Abstract

Mechanical properties of composites made up of high-density polyethylene (HDPE) and silanated TiO_2 particles for use as a bone-repairing material were investigated in comparison with those of the composites of HDPE with unsilanized TiO_2 particles. The interfacial morphology and interaction between silanated TiO_2 and HDPE were analyzed by means of Fourier transform infrared (FT-IR) spectroscopy and scanning electron microscopy (SEM). The absorption in spectral bands related to the carboxyl bond in the silane-coupling agent, the vinyl group in the HDPE, and the formation of the ether bond was studied in order to assess the influence of the silane-coupling agent. The SEM micrograph showed that the "bridging effect" between HDPE and TiO_2 was brought about by the silane-coupling agent. The use of the silane-coupling agent and the increase of the hot-pressing pressure for shaping the composites facilitated the penetration of polymer into cavities between individual TiO_2 particles, which increased the density of the composite. Therefore, mechanical properties such as bending yield strength and Young's modulus increased from 49 MPa and 7.5 GPa to 65 MPa and 10 GPa, respectively, after the silane-coupling treatment and increase in the hot-pressing pressure.

Keywords: A. Composites; C. Infrared spectroscopy; D. Mechanical property

1. Introduction

Since the discovery of Bioglass® in the early 1970s [1], various bioactive ceramics, including sintered hydroxyapatite [2] and glass–ceramic A-W containing crystalline apatite and wollastonite ($CaO{\cdot}SiO_2$) [3], have been developed and clinically used as materials, for example, for artificial middle-ear bones, maxillofacial implants, bone fillers, artificial iliac crests, artificial vertebrae, and artificial intervertebral discs. Among them, glass–ceramic A-W shows fracture toughness as high as 2 MPa $m^{1/2}$ [4,5] and high bioactivity [6]. Hence it can be used to replace bones subjected to high loads, such as vertebrae and intervertebral discs [7]. Highly loaded bones such as tibial and femoral bones, however, cannot be replaced even with this glass–ceramic, since its fracture toughness is lower and its elastic modulus is higher than those of natural bone. For these purposes, implants made of metal, such as titanium metal and

* Corresponding author. Tel.: +81 52 871 3500; fax: +81 52 871 3599.
E-mail addresses: masami@jfcc.or.jp (M. Hashimoto), takadama@jfcc.or.jp (H. Takadama), mizuno@jfcc.or.jp (M. Mizuno), kokubo@isc.chubu.ac.jp (T. Kokubo).
[1] Tel.: +81 568 51 6583; fax: +81 568 51 1642.

0025-5408/$ – see front matter
doi:10.1016/j.materresbull.2005.09.014

its alloy, subjected to alkali and heat treatment [8] or alkali, water and heat treatment [9] have been developed. They have, however, much higher elastic moduli than that of natural bone. This is a critical problem in some applications, since the high elastic modulus of these materials may induce resorption of the surrounding bone because of stress shielding. Therefore, highly bioactive materials with mechanical properties analogous to those of natural bone are desired to be developed.

Hydroxyapatite-particle-reinforced high-density polyethylene (HDPE) composite (HAPEX®) was developed in the early 1980s as an analogue for bone [10]. It is already in clinical use as the material of artificial middle-ear bones. Some of the mechanical properties of HAPEX®, such as the tensile strength, have already been confirmed to be suitable for use in the human body [11–13]. However, the fracture toughness and elastic modulus of HAPEX® are lower than those of living bone. Glass–ceramic A-W-reinforced HDPE has been in development since 1998 [14,15]. The bioactivity of this composite is higher than that of HAPEX®, but the mechanical strengths of this composite are lower.

Previous studies by the present authors have shown that TiO_2-nanoparticle-reinforced HDPE composites (hereafter TiO_2/HDPE) exhibit bending strength and Young's modulus analogous to those of natural bone as well as bioactivity [16,17]. The bending strength and Young's modulus were found to vary from almost 28 to 54 MPa and 1.4 to 7.6 GPa, respectively, depending on the TiO_2 content. However, only a very weak mechanical adhesion seemed to exist between constituent phases in these composites. The fracture surface of the TiO_2/HDPE composites showed no residual HDPE on the TiO_2 particles, indicating that no chemical bond existed between TiO_2 and HDPE. Also, there were voids at the particle–matrix interface, resulting in a lower density than the theoretical one.

For incompatible composites containing at least one component, the final mechanical strengths are determined by two competing factors. One is the extent of compatibility between the inorganic filler and the polymer. The other is the presence of voids, cracks and fractures in the interphase between the filler and polymer [18].

The interface between inorganic filler particles and the matrix polymer plays an important role in determining the properties of a composite. Particle–matrix interaction is expected to influence the structure of the composites, mainly through its influence on the dispersion of the filler particles in the matrix [19–21]. Most commonly, the surface of the filler is treated to become more chemically compatible with the polymer matrix. A very common reactive treatment is silane treatment of the fillers [22]. The widespread use of silane treatment can be attributed to the availability of a wide range of endgroups. Thus, the interaction between the inorganic surface and the matrix polymer can be tuned by selecting the appropriate endgroups.

In this work, we focus on the study of composites of HDPE and surface-modified TiO_2, in particular, the adhesion between the two phases. The silane molecule used for surface treatment has the hydrocarbon functional group. The hydrocarbon endgroup is used in coupling agents that interact well with polyolefin, such as polyethylene. Also, the synergistic effects of surface treatment and of the increase of hot-pressing (HP) pressure applied during shaping on mechanical strength were investigated.

2. Experimental

2.1. Materials

Solvents and reagents, all of special reagent grade, were used without further purification. The anatase-type TiO_2 nanopowder was manufactured by Ishihara Sangyo Kaisha, Ltd., Mie, Japan. The median particle size of TiO_2 powders was 535 nm [17]. TiO_2 powders were treated with a silane-coupling agent as follows: 1.1 g of [γ-(methacryloxy)propyl]trimethoxysilane (γ-MPS) (Shinetsu Co. Ltd., Osaka, Japan), 1.6 g of ethanol and 0.2 g of ion-exchanged distilled water were stirred with a magnetic stirrer for 10 min. The solution containing the silane-coupling agent was added to 110 g of TiO_2 powder and mixed in the shaker mixer TURBULA T2F (W. A. Bachofen AG Co., Basel, Switzerland) at 25 °C for 1 h. The rotation speed was 96 rpm. After mixing, the mixtures were dried and heated at 130 °C for 5 min.

HDPE (Japan Polyolefins Co., Ltd., Tokyo, Japan) has the number-average molecular weight (Mn) of 1.21×10^4, weight-average molecular weight (Mw) of 7.67×10^4 and z-average molecular weight (Mz) of 47.6×10^4; Mw/Mn is 6.35 and Mz/Mw is 6.20. The melt flowing rate (MFR) of this polyethylene is 8.

The influence of silanation of TiO_2 nanoparticles on the flow behavior of TiO_2/HDPE compound was evaluated using a computer-controlled torque rheometer, 30C-150 (Toyo Seiki Seisaku-sho, Ltd., Tokyo, Japan). Reaction was performed in a chamber with continuous monitoring of torque. The mixer chamber was initially heated to 210 °C.

HDPE and TiO_2 with and without γ-MPS treatment were introduced into the heated chamber simultaneously. The rotor speed was fixed at 25 rpm. The total mixing process lasted about 30 min.

2.2. Preparation of TiO_2/HDPE composites

The manufacturing process of TiO_2/HDPE with γ-MPS involved kneading and compression molding. The filler content was set at 40 vol% because the composite with this composition shows both bioactivity and mechanical properties analogous to those of human cortical bone [17]. This composite was denoted as TiO_2/HDPE-40. HDPE was dried at 80 °C for 8 h and then kneaded at 210 °C in a batch kneader PBV 0.3 (Irie Shokai, Ltd., Tokyo, Japan). TiO_2 particles were added slowly into the melted HDPE with kneading at 210 °C in air. After adding TiO_2, TiO_2/HDPE compound was kneaded at 25 rpm for 30 min.

The obtained compounds were molded at 230 °C for 1 h and then hot-pressed in air at pressures between 2.5 and 5.8 MPa. TiO_2/HDPE composite without γ-MPS was also produced via the same route for comparison purposes.

2.3. Characterization of TiO_2/HDPE composites

2.3.1. Fourier transform infrared spectroscopy

The spectra of the TiO_2/HDPE-40 composite with and without γ-MPS hot-pressed at 2.5 MPa were analyzed with a FT-IR spectrophotometer FT/IR-550 (JASCO Co., Osaka, Japan). The hot-pressed composite surface was ground and dispersed in a matrix of KBr, followed by compression to consolidate the formation of the pellet. FT-IR spectra were obtained by the KBr pellet method in the wave-number range from 400 to 4000 cm^{-1} with a resolution of 4 cm^{-1}.

2.3.2. SEM observation

The fracture surfaces of TiO_2/HDPE-40 composites with and without γ-MPS hot-pressed at 2.5 MPa were examined using the field emission scanning electron microscope (FE-SEM) JSM-633OF (JEOL DATUM Co. Ltd., Nagoya, Japan) after coating them with a thin Au film.

2.3.3. Mechanical test

Three-point bend testing was performed using five samples of each type of composite. The specimens were cut to the desired shape and then polished, using 400 grit silicon carbide paper, to a size of 40 mm × 10 mm × 4 mm. A testing machine, Model 5582 (Instron Co. Ltd., LA, USA), was used to apply a load over a 30 mm span. Measurements were performed with a cross-head speed of 1.0 mm/min at room temperature, according to JIS K 7171. Bending yield strength was calculated as [14,23]

$$\text{Bending yield strength,}\quad \sigma_f = \left(\frac{3p_fL}{2bd^2}\right)\left(\frac{n+2}{3}\right) \tag{1}$$

p_f is the load at fracture (N), L is the sample length (mm), b is the sample width (mm), d is the sample height (mm), and n is a strain-hardening exponent ($0 < n < 1$). The strain-hardening exponent n was estimated as the slope of log–log plot of p versus δ in the nonlinear region of the load–displacement curve. δ is the deflection of the specimen at mid-span (mm).

The Young's modulus was estimated from the slope of the initial linear elastic region of the load–displacement curve.

2.3.4. Density

The density of TiO_2/HDPE-40 composite was measured by the Archimedes method using a pycnometer and a glass bottle of known volume with a capillary tube at the top as a container. The liquid medium was distilled water for all materials.

3. Results

3.1. Torque of composites

It is known that melt viscosity can be related to the torque measured by the equipment during blending [24]. Fig. 1 shows a plot of torque versus time for TiO_2/HDPE-40 with (a) and without (b) γ-MPS. The introduction of cold HDPE

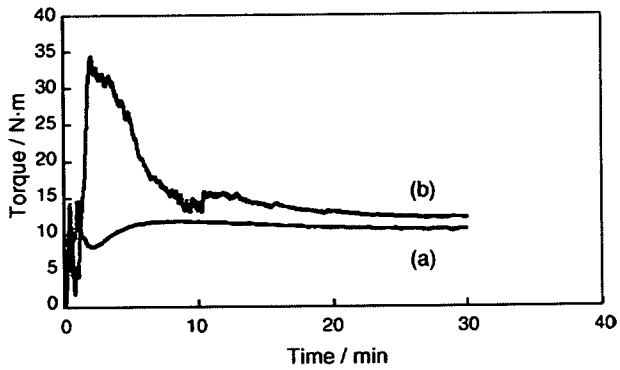

Fig. 1. Plot of torque vs. time for TiO_2/HDPE-40 composites with (a) and without (b) γ-MPS at 200 °C.

and TiO_2 into the preheated mixer chamber initially led to an increase of torque, followed by a decrease of torque during the fusion of HDPE (Fig. 1(a) and (b)). The torque of TiO_2/HDPE-40 without γ-MPS became approximately constant after about 10 min (Fig. 1(b)). On the other hand, the system containing γ-MPS showed lower and variable torque during experiments (Fig. 1(a)). The addition of γ-MPS decreased the torque during the first 2–3 min due to the plasticizing effect of the silanized TiO_2. This torque slowly increased with processing, probably due to chain branching reactions induced by heat and mechanical forces. The torque of TiO_2/HDPE-40 composite with γ-MPS was lower than that of composite without γ-MPS after blending for 30 min. Therefore, a silane-coupling agent such as γ-MPS produced a lower viscosity TiO_2/HDPE-40 composite, as can be seen from curve (a).

3.2. FT-IR spectra of composites

Fig. 2 shows the characteristic spectra of TiO_2/HDPE-40 with (a) and without (b) γ-MPS. It shows the bands involved in the interfacial interaction between the TiO_2 particles and the HDPE matrix in the presence or absence of γ-MPS. Upon comparing the composite spectra, differences in the shape and position of the bands can be observed.

The most significant bands of the TiO_2 particles studied and the assignment for each one are a broad adsorption band between 500 and 1000 cm^{-1} attributed to Ti–O–Ti linkages in TiO_2 nanoparticles [25,26]. On the other hand, in the HDPE spectrum, it is necessary to highlight the band at 1474 cm^{-1} ($-CH_2$) [27] and the characteristic band at 1386 cm^{-1} (wagging $-CH_2$) [27]. In Fig. 2, one special band at 1720 cm^{-1} and a slightly different shape at 900–1300 cm^{-1}, corresponding to neither TiO_2 particles nor HDPE, are observed only for the composite with γ-MPS (a). Also, the bands at 3085 cm^{-1} and 3025 cm^{-1} are observed for the composite without γ-MPS (b).

Fig. 3 shows the FT-IR spectra in the 1300–2000 cm^{-1} region of the TiO_2/HDPE-40 composite hot-pressed at 2.5 MPa with (a) and without (b) γ-MPS. As shown in Fig. 3(a), the spectral band at 1720 cm^{-1} was attributed to the carboxyl group of γ-MPS. This result indicates the applicability of silane coupling on the surface of TiO_2 particles. The spectral band at 1654 cm^{-1} corresponds to water absorption due to the hydrophilic character of the TiO_2 particles (Fig. 3(a) and (b)).

Fig. 4 shows the FT-IR spectra in the 900–1300 cm^{-1} region of the TiO_2/HDPE-40 composite hot-pressed at 2.5 MPa with (a) and without (b) γ-MPS. The spectral band at 1162 cm^{-1} was attributed to an ether bond (C–O–C). Also, two broad bands appear at 1106 and 1035 cm^{-1}, which are assigned to Si–O stretching vibration, indicating the generation of a Si–O–Si network [28]. The absorption peak at about 940 cm^{-1} corresponds to Si–O–Ti stretching vibration [29,30].

Fig. 5 shows the FT-IR spectra in the 2700–3300 cm^{-1} region of the TiO_2/HDPE-40 composite hot-pressed at 2.5 MPa with (a) and without (b) γ-MPS. The 2946 cm^{-1} band is assigned to the symmetric stretching of CH_2 in HDPE for composites containing 40 vol% of TiO_2 (Fig. 5(a) and (b)). The bands at 3085 and 3025 cm^{-1}, corresponding to the bending of the vinyl group in HDPE, are reduced in the case of TiO_2/HDPE-40 with γ-MPS (Fig. 5(a)).

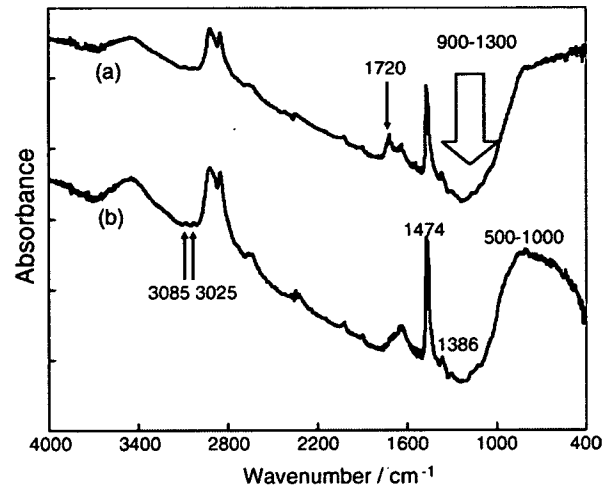

Fig. 2. FT-IR spectra of TiO_2/HDPE-40 composites with (a) and without (b) γ-MPS.

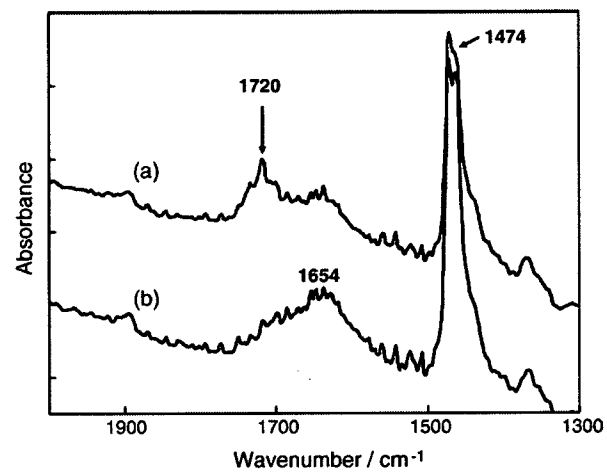

Fig. 3. FT-IR spectra in the 1300–2000 cm^{-1} region for TiO_2/HDPE-40 composites with (a) and without (b) γ-MPS.

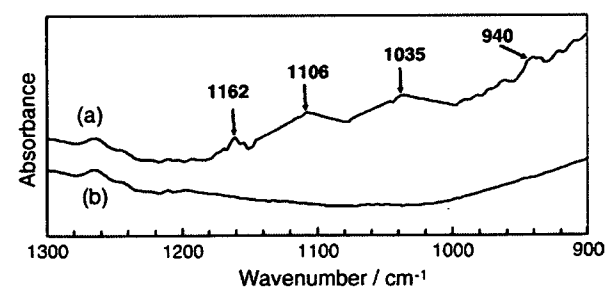

Fig. 4. FT-IR spectra in the 900–1300 cm^{-1} region for TiO_2/HDPE-40 composites with (a) and without (b) γ-MPS.

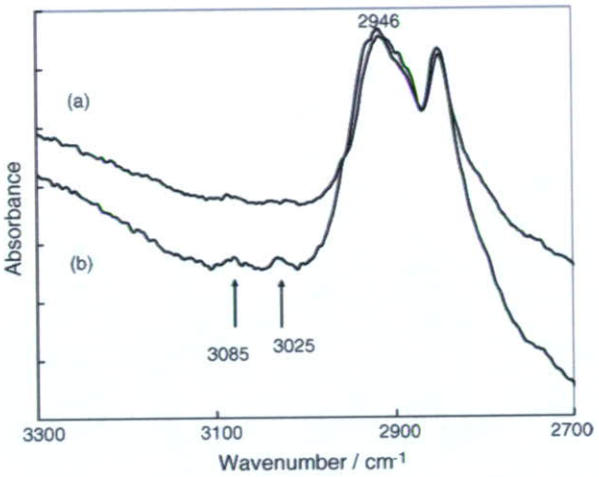

Fig. 5. FT-IR spectra in the 2700–3300 cm^{-1} region for TiO_2/HDPE-40 composites with (a) and without (b) γ-MPS.

3.3. SEM characterization of composites

Fig. 6 shows FE-SEM images of the fracture surfaces of TiO_2/HDPE-40 with (a) and without (b) γ-MPS after the bending test. This figure shows the effect of a tensile load on local deformation of HDPE around the TiO_2 particles in each of the composites. As the FE-SEM image in Fig. 6(a) shows, HDPE covered the surface of individual TiO_2 particles, indicating that a chemical bond existed between TiO_2 and HDPE. However, for TiO_2/HDPE without γ-MPS (Fig. 6(b)), no residual HDPE was found on the TiO_2 particles.

3.4. Mechanical properties of composites

The bending yield strength and Young's modulus of TiO_2/HDPE-40 with (a) and without (b) γ-MPS as a function of hot-pressing (HP) pressure are shown in Figs. 7 and 8, respectively. In the case of TiO_2/HDPE-40 without γ-MPS, the bending yield strength and Young's modulus were independent of HP pressure (Figs. 7(b) and 8(b)). On the other hand, the bending yield strength and Young's modulus of TiO_2/HDPE-40 with γ-MPS increased with increasing HP pressure up to 5 MPa and decreased at pressures higher than 5.7 MPa. The bending yield strength and Young's modulus, respectively, were 49 MPa and 7.5 GPa for the HP pressure of 2.5 MPa, 58 MPa and 8 GPa for the HP pressure of 4.5 MPa, 65 MPa and 10 GPa for the HP pressure of 5 MPa, and 61 MPa and 7 GPa for the HP pressure of 5.7 MPa.

The representative load–displacement curves were obtained for HDPE, and TiO_2/HDPE-40 without (Fig. 9) and with γ-MPS (Fig. 10) by three-point bend testing. Pure HDPE did not fracture within the limits of the three-point

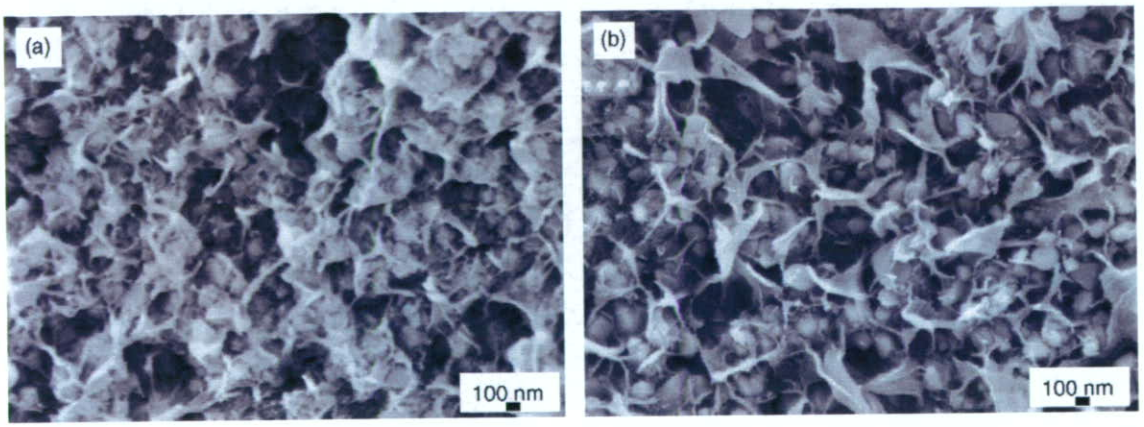

Fig. 6. Scanning electron micrographs of fracture surfaces of TiO_2/HDPE-40 composites with (a) and without (b) γ-MPS.

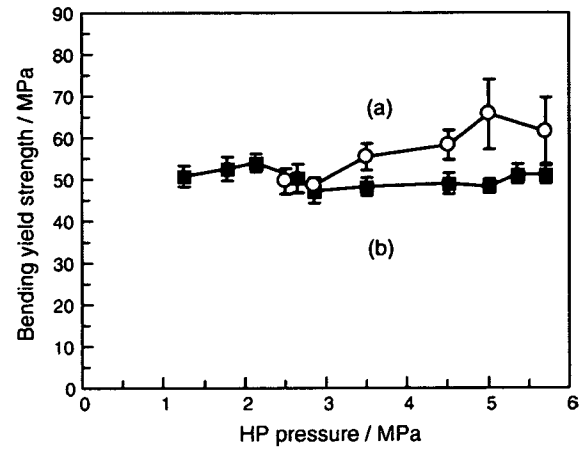

Fig. 7. Bending yield strength of TiO_2/HDPE-40 composites with (a) and without (b) γ-MPS as a function of hot-pressing pressure.

bending apparatus. This behavior indicated the mechanical properties of low bending yield strength and Young's modulus, and large strain to failure. For TiO_2/HDPE-40 without γ-MPS (Fig. 9), it can be noted that all the curves exhibit nearly linear behavior independent of HP pressure. All the composites break in a brittle manner when the load reaches a maximum. However, for TiO_2/HDPE-40 with γ-MPS (Fig. 10), all the curves exhibit the non-linear behavior of a ductile matrix. Once the load reaches its maximum value there are clearly significant differences in the way these

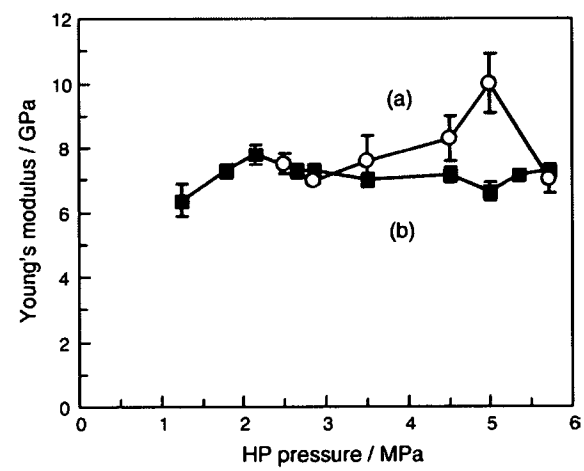

Fig. 8. Young's modulus of TiO_2/HDPE-40 composites with (a) and without (b) γ-MPS as a function of hot-pressing pressure.

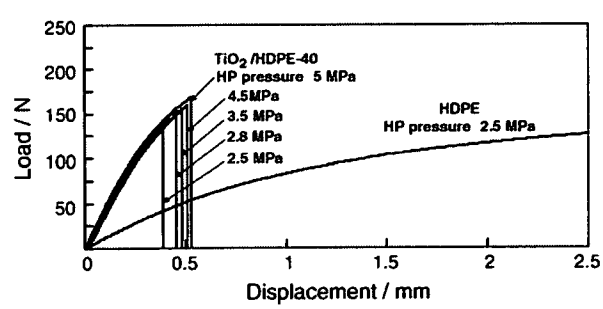

Fig. 9. Load–displacement curve of TiO_2/HDPE-40 composite without γ-MPS hot-pressed at various pressures and that of pure HDPE.

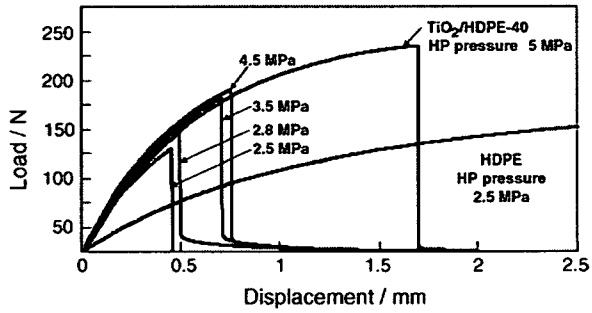

Fig. 10. Load–displacement curve of TiO_2/HDPE-40 composite with γ-MPS hot-pressed at various pressures and that of pure HDPE.

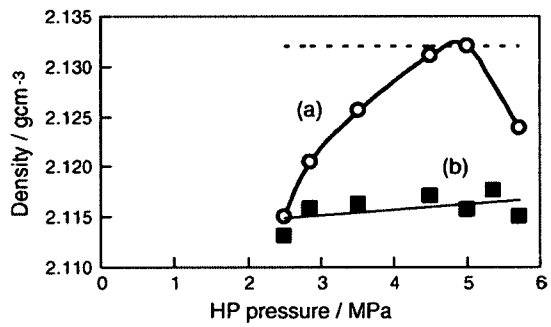

Fig. 11. Density of TiO_2/HDPE-40 composite with (a) and without (b) γ-MPS as a function of pressure applied during shaping (dotted line represents the theoretical density value of 2.132 g/cm^3).

curves decrease. The load–displacement curve depicts a weakly bonded interphase after the interphase fails (HP pressure 2.5 MPa). The TiO_2 particles were separated from the matrix in a controlled manner and friction was measured until all TiO_2 particles were completely removed (HP pressure: 2.8, 3.5 and 4.5 MPa). Fig. 10 shows that the load–displacement curve for silane-treated composite (HP pressure 5 MPa) indicates a very strongly bonded interphase; the interface failed immediately after complete TiO_2 particle separation.

3.5. Density of composites

Fig. 11 shows the densities of the TiO_2/HDPE-40 composites with (a) and without (b) γ-MPS as a function of HP pressure. Compared with the theoretical density (denoted by the dotted line), which was calculated using the rule of mixture, the density of TiO_2/HDPE with γ-MPS (a) increased with HP pressure up to almost identical value to the theoretical one (2.132 g/cm^3) at 5 MPa. However, as the hot-pressing pressure was increased to 5.7 MPa, the discrepancy between the measured and theoretical densities increased. In contrast, the density of TiO_2/HDPE without γ-MPS (b) was independent of HP pressure.

4. Discussion

The mechanical strength of TiO_2/HDPE-40 was enhanced by both the silanation of TiO_2 and the increase of the HP pressure applied to shape the composite.

The TiO_2/HDPE composite without γ-MPS presents very weak physicomechanical adhesion, as shown in Fig. 6(b). For the fracture surface of the TiO_2/HDPE composite, no residual HDPE was found on the TiO_2 particles, indicating that no chemical bond existed between the matrix and filler. Therefore, the voids form at the particle–matrix interface, first in the direction of the applied stress. This void then grows and merges as shear stresses deform the rest of the matrix, leading to the eventual failure of the composites. This result was consistent with the model proposed by Juhasz et al. for an apatite–wollastonite-reinforced HDPE composite with no interfacial bonding [15]. Hence stress transfer

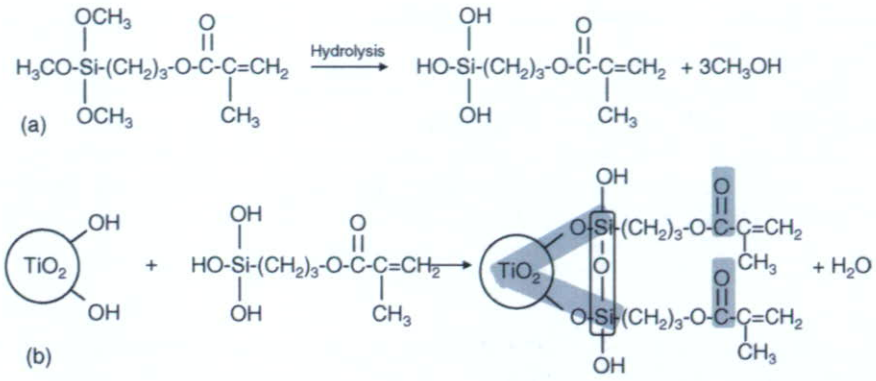

Fig. 12. Scheme of hydrolyzation of γ-MPS and absorption of hydrolyzed alkoxysilanol on TiO_2.

does not take place between TiO_2 and HDPE. On the other hand, for the silanated TiO_2/HDPE composite, as shown in Fig. 6(a), the silane-coupling agent facilitates direct contact between the TiO_2 particles and the HDPE matrix to a higher degree than the contact in the untreated composite. It can also be observed that the composites broke due to shear yield and tearing. The differences between the failure surfaces of differently treated composites are attributed to the different chemical natures of the coupling agent and the different adhesion mechanisms.

In the silanated TiO_2/HDPE composite, as shown in Fig. 4(a), the bands of 1035 and 1106 cm^{-1} are mainly attributed to Si–O–Si vibration. The silane-coupling agent undergoes chemical changes during hydrolysis and drying. During hydrolysis of the silane, the $SiOCH_3$ group will transform into SiOH, as shown in Fig. 12(a). Then, the hydrolyzed alkoxysilanol can be absorbed into the surface and condenses with the hydroxyl group of TiO_2 components, as shown in Fig. 12(b). The hydrolyzed alkoxy silanes can undergo condensation and bond formation. Besides these reactions of the silanol and the hydroxyl groups of the TiO_2 surface, the formation of the siloxane structure can also occur, which gives rise to the band at 940 cm^{-1} attributed to Si–O–Ti (Fig. 4(a)). This reveals the formation of a covalent bond between the silane-coupling agent and the TiO_2 particles.

Fig. 5 shows the evolution of the reduced absorbance corresponding to the bending of the vinyl group (–CH=CH_2, 3025 and 3085 cm^{-1}). This seems to correspond to the reactivity between the double bond of HDPE and those of the coupling agent on TiO_2 particles, as shown in Fig. 13. Therefore, HDPE covered the surface of individual TiO_2 particles, as shown in Fig. 6(a).

Homogeneous dispersion of nanoparticles in a polymeric matrix is very difficult due to the strong tendency of nanoparticles to agglomerate. Consequently, the so-called nanoparticle-filled polymers sometimes contain a number of loosened clusters of particles. It can be seen that in the silane-treated composite, HDPE penetrated into the cavity between TiO_2 particles because of its low viscosity in the molten state (Fig. 1). This seems to indicate that wetting of the TiO_2 particles plays a key role in TiO_2 and HDPE matrix adhesion because it increases the degree of mechanical

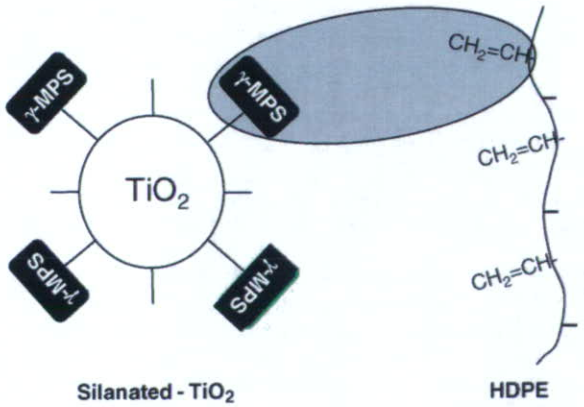

Fig. 13. Adhesion mechanism for silane-treated TiO_2 and HDPE.

interlocking. This means that proper TiO_2 wetting by γ-MPS and an increased hot-pressing pressure could explain the increment of the density of the composites (Fig. 11(a)).

These studies revealed that the final mechanical strengths are determined by two competing factors: one is the increase in compatibility between TiO_2 and HDPE due to the presence of the silane-coupling agent, and the other is the increase in the density of the composite. Also, with high strain (pressure applied during shaping is higher than 5 MPa), the properties of the composite seemed to be deteriorated because high strain leads to the formation of cracks and fractures at interphase boundaries. Therefore, the mechanical strengths of TiO_2/HDPE composite decreased due to the decrease of density.

5. Conclusions

The bending yield strength and Young's modulus increased with the increase of the pressure applied during shaping only for the silane-treated TiO_2/HDPE composite (maximum bending yield strength = 65 MPa, Young's modulus = 10 GPa). γ-MPS has a higher capacity to form the covalent bond, that is, an ether bridge (1162 cm^{-1}). The vinyl groups of HDPE reacted with the double bonds within γ-MPS. Increasing the pressure applied during shaping resulted in an increase in the density of silane-treated TiO_2/HDPE composite. These chemical interactions between TiO_2 and HDPE and the disappearance of voids and cracks resulted in better mechanical performance of silane-treated TiO_2/HDPE composite.

Acknowledgement

This work is supported in part by the National Research and Development Programs for Medical and Welfare Apparatus entrusted by the New Energy and Industrial Technology Development Organization (NEDO) to the Japan Fine Ceramics Center.

References

[1] L.L. Hench, R.J. Splinter, W.C. Allen, T.K. Greenlee Jr., J. Biomed. Mater. Res. 2 (1971) 117–141.
[2] M. Jarcho, J.L. Kay, R.H. Gumaer, H.P. Drobeck, J. Bioeng. 1 (1977) 79–92.
[3] T. Kokubo, M. Shigematsu, Y. Nagashima, M. Tashiro, T. Nakamura, T. Yamamuro, S. Higashi, Bull. Inst. Chem. Res. Kyoto Univ. 60 (1982) 260–268.
[4] T. Kokubo, S. Ito, M. Shigematsu, S. Sakka, T. Yamamuro, J. Mat. Sci. 20 (1985) 2001–2004.
[5] T. Kokubo, S. Ito, M. Shigematsu, S. Sakka, T. Yamamuro, J. Mat. Sci. 22 (1987) 4067–4070.
[6] K. Ono, T. Yamamuro, T. Nakamura, T. Kokubo, Biomaterials 11 (1990) 265–271.
[7] T. Yamamuro, J. Shikata, H. Okumura, T. Kitsugi, Y. Kakutani, T. Matsui, T. Kokubo, J. Bone Joint Surg. 72-B (1990) 889–893.
[8] H.M. Kim, F. Miyaji, T. Kokubo, T. Nakamura, J. Biomed. Mater. Res. 32 (1996) 409–417.
[9] M. Uchida, H.M. Kim, T. Kokubo, S. Fujibayashi, T. Nakamura, J. Biomed. Mater. Res. 63 (5) (2002) 522–530.
[10] W. Bonfield, M.D. Grynpas, A.E. Tully, J. Bowman, J. Abram, Biomaterials 2 (1981) 185–186.
[11] M. Wang, R. Joseph, W. Bonfield, Biomaterials 19 (1998) 2357–2366.
[12] M. Wang, W. Bonfield, Biomaterials 22 (2001) 1311–1320.
[13] M. Wang, Biomaterials 24 (2003) 2133–2151.
[14] J.A. Juhasz, S.M. Best, W. Bonfield, M. Kawashita, N. Miyata, T. Kokubo, T. Nakamura, J. Mater. Sci.—Mater. Med. 14 (2003) 489–495.
[15] J.A. Juhasz, S.M. Best, R. Brooks, M. Kawashita, N. Miyata, T. Kokubo, T. Nakamura, W. Bonfield, Biomaterials 25 (2004) 949–955.
[16] H. Takadama, M. Hashimoto, Y. Takigawa, M. Mizuno, Y. Yasutomi, T. Kokubo, Key Eng. Mater. 254–256 (2004) 569–572.
[17] M. Hashimoto, H. Takadama, M. Mizuno, T. Kokubo, J. Mater. Sci.—Mater. Med., Submitted for publication.
[18] S. Jose, A.S. Aprem, B. Trancis, M.C. Chandy, P. Werner, V. Alstaedt, S. Thomas, Eu. Polym. J. 40 (2004) 2105–2115.
[19] B. Pukanszky, E. Fekete, F. Tudos, Chemie Macromolecular Symposia 28 (1989) 165–186.
[20] J. Jancar, J. Kucera, Polym. Eng. Sci. 30 (12) (1990) 707–713.
[21] J. Jancar, J. Kucera, Polym. Eng. Sci. 30 (12) (1990) 714–720.
[22] E.P. Plueddemann, Silane Coupling Agents, 3rd ed., Plenum Press, New York, 1991.
[23] N.E. Dowling (Ed.), Engineering Materials For Deformation, Fracture and Fatigue, Prentice-Hall Inc., Englewood Cliffs, NJ, 1993, pp. 570–617 (Chapter 13).
[24] F.W. Fabris, F.C. Stedile, R.S. Mauler, S.M.B. Nachtigall, Eu. Polym. J. 40 (2004) 1119–1126.
[25] C. Xie, Z. Xu, Q. Yang, B. Xue, Y. Du, J. Zhang, Mater. Sci. Eng., B 112 (2004) 34–41.
[26] T. Bezrodna, G. Puchkovska, V. Shymanovska, J. Baran, H. Ratajczak, J. Mol. Struct., in press.
[27] X. Colom, F. Carrasco, P. Pages, J. Canavate, Compos. Sci. Technol. 63 (2003) 161–169.
[28] B.B. Johnsen, K. Olafsen, A. Stori, Int. J. Adhes. Adhes. 23 (2003) 155–163.
[29] B. Bai, J. Zhao, X. Feng, Mater. Lett. 57 (2003) 3914–3918.
[30] G. Gu, Z. Zhang, H. Dang, Appl. Surf. Sci. 221 (2004) 129–135.

Key Engineering Materials Vols. 309-311 (2006) pp. 797-800
online at http://www.scientific.net

Bioactive PMMA-Based Cement Incorporated with Nano-Sized Rutile Particles

M. Hashimoto[1, a], H. Takadama[1, b], M. Mizuno[1, c], T. Kokubo[2, d], K. Goto[3, e] and T. Nakamura[3, f]

[1]Japan Fine Ceramics Center, 2-4-1 Mutsuno, Atsuta-ku, Nagoya 456-8587, Japan

[2]Research Institute for Science and Technology, Chubu University, Kasugai, Japan

[3]Faculty of Medicine, Kyoto University, Kyoto Japan

[a]masami@jfcc.or.jp, [b]takadama@jfcc.or.jp, [c]mizuno@jfcc.or.jp, [d] kokubo@isc.chubu.ac.jp, [e]k.g.bau@kuhp.kyoto-u.ac.jp, [f]ntaka@kuhp.kyoto-u.ac.jp

Keywords: rutile; mechanical strength; apatite; simulated body fluid; polymethylmethacrylate

Abstract

Bioactive bone cement with mechanical properties higher than that of commercial polymethylmethacrylate (PMMA) bone cement are strongly desired to be developed. In the present study, PMMA-based cement incorporated with nano-sized rutile particles was prepared. The PMMA-based cement (rutile content was 50 wt%) shows the compressive strength (136 MPa) higher than that of commercial PMMA bone cement (88 MPa). The hardened cement formed apatite on the surface in a simulated body fluid within 3 days. Therefore, this PMMA-based cement incorporated with rutile particles might be useful as cement for fixation of prostheses as well as self-setting bone substitutes, because of its high apatite forming ability and mechanical strength.

Introduction

Various types of bioactive bone cements have been proposed to overcome the disadvantages of polymethylmethacrylate (PMMA) bone cement, such as lack in bone-bonding ability, which occasionally leads to aseptic loosening of prosthesis for arthroplasty [1-3]. And also, it is beset with some well-known disadvantages such as its high polymerization exotherm and brittle nature.

The present authors previously tried to prepare bioactive PMMA-based cement by incorporation of nano-sized anatase particles [4]. The anatase particles, however, were not uniformly dispersed in the cement, since they were aggregated.

In the present study, preparation of bioactive PMMA-based cement was attempted by incorporation of nano-sized rutile particles. It is already reported that not only anatase but also rutile form apatite on their surfaces in a simulated body fluid (SBF) [5], and that materials which form the apatite on their surfaces in SBF bond to living bone through the apatite formed on their surfaces in the living body. The purpose of the present study was to evaluate the setting and mechanical properties, and apatite forming ability in the SBF of the PMMA-based cement with nano-sized rutile particles.

Materials and methods

Cement preparation

PMMA beads 5 μm in average diameter (Sekisui Plastics Co. Ltd, Shiga, Japan, Mw 270,000) were mixed with rutile particles 300 nm in average size (Ishihara Sangyo Kaisha, Ltd., Osaka, Japan) and benzoyl peroxide (BPO) powders (Nacalai Tesque, Inc., Kyoto, Japan) in the shaker mixer TURBULA T2F (W. A. Bachofen AG Co., Basel, Switzerland) at 25 °C for 15 min. The rotation speed was 96 rpm. Methylmethacrylate (MMA) monomer liquid (Wako Pure Chemical Industries,

Ltd., Osaka, Japan) was mixed with N, N-dimethyl-p-toluidine (DMPT) liquid (Kanto Chemical Co. Inc., Tokyo, Japan). The former powder was mixed with the later liquid at powder to liquid in weight ratio of 7 / 3. Rutile content was 50 wt %. MMA to PMMA weight ratio was 0.92. BPO and DMPT were 4.0 and 2.0 wt% of MMA, respectively. Commercial PMMA cement (CMW1, DePuy International Ltd. Blackpool, England) was used as a reference.

Setting time and maximum temperature

Approximately 25 g of the mixed paste was cast into a Teflon mould 60 mm in diameter and 20 mm in depth. Temperature variation during the setting reaction of the cement paste was monitored by infrared-radiated thermometer under ambient conditions of 23 °C and 45-56 % humidity. The setting time was defined as the time when the temperature reached a half difference between the room temperature and the maximum temperature.

Mechanical testing

For compressive mechanical analysis, the mixed paste was cast into the Teflon mould 12 mm in depth and 6 mm in diameter. The hardened cement was extruded and cylindrical specimen abraded with 400 grit silicon carbide papers to remove defects from the specimen surfaces. The strength was measured at a cross-head speed of 4 mm/min at room temperature in air, according to ISO 5833.

SBF soaking

Plate specimens 15 x 10 x 4 mm^3 in size were cut from the hardened cement and soaked in 30 ml of SBF with ion concentrations (Na^+ 142.0, K^+ 5.0, Mg^{2+} 1.5, Ca^{2+} 2.5, Cl^- 147.8, HCO_3^- 4.2, HPO_4^{2-} 1.0, SO_4^{2-} 0.5 mM) nearly equal to those of human blood plasma [6] at 36.5 °C for various periods. After removal from the SBF, the specimens were washed with distilled water and dried in the air. Surface structural changes of the specimens were examined by field emission scanning electron microscope (FE-SEM) and thin-film X-ray diffraction.

Results and discussion

The mixed paste containing the rutile particles facilitates lower viscosity compared to the paste containing the anatase. The maximum temperature during the setting reaction was 87 °C for the present cement whereas 100 °C for the commercial PMMA cement. The lower polymerization exotherm and the lower viscosity of the present cement allowed better handling property. The setting time was 18 min for the present cement whereas 10 min for the commercial PMMA cement. The setting time varied depending on the MMA to PMMA weight ratio.

Figure 1 shows the representative load-displacement curves for compressive testing of the present cement and the commercial PMMA cement. The increase of flow load for rutile-incorporated PMMA cement is evident. The present cement had larger effective fracture energy than commercial PMMA cement. This kind of material which do not break off but deform to some extent and absorb the fracture energy even under highly loaded condition are desirable for bone cement. The compressive strength was 136 MPa for the present cement whereas 88 MPa for the commercial PMMA cement.

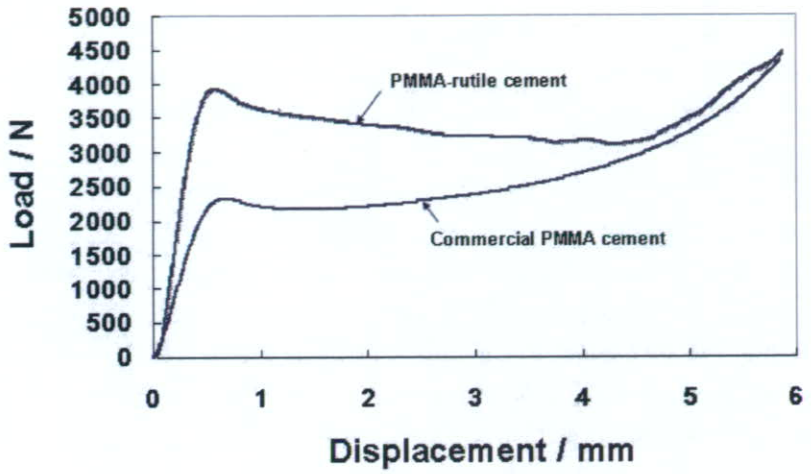

Fig. 1 The load-displacement curves for compressive testing of PMMA-rutile cement and commercial PMMA cement.

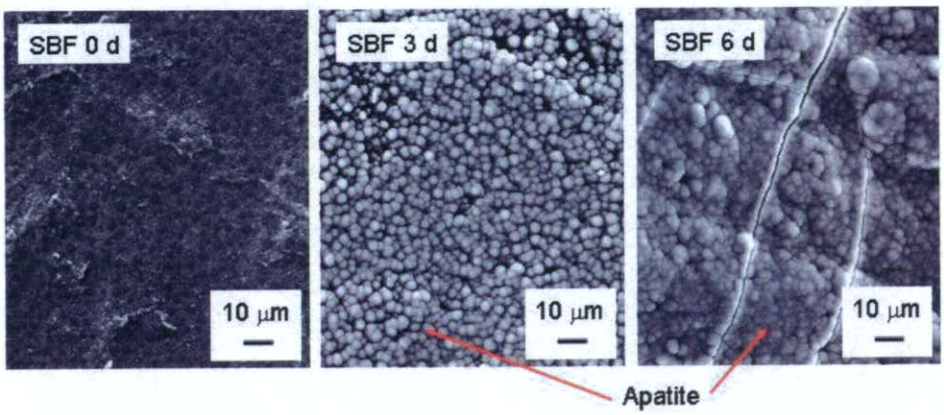

Fig. 2 Scanning electron micrographs of the surfaces of the PMMA-rutile cement soaked in SBF at 36.5 °C for various periods.

Figure 2 shows FE-SEM photographs of the present cement soaked in SBF at 36.5 °C for various periods up to 6 days. The present cement was covered with hemispherical particles around several micrometers in diameter after 3 days of soaking in SBF. TF-XRD patterns of the present cement shows this particles are the bone-like apatite. The number of the apatite nuclei increased with increasing soaking time within 6 days, whereas the commercial PMMA cement was not formed with the apatite on its surface even after 14 days.

Conclusions

The PMMA-based cement incorporated with nano-sized rutile particles was prepared by simple hand mixing of the liquid and powder. This cement improved handling properties and lower polymerization exotherm. The PMMA-rutile cement (rutile content was 50 wt%) showed higher compressive strength than commercial PMMA cement. The present cement formed apatite on this surface in SBF within 3 days. Therefore, this cement is considered to be useful as cement for fixation of prostheses as well as self-setting bone substitute.

Acknowledgements

This work is in part supported by the National Research & Development Programs for Medical and Welfare apparatus from the New Energy and Industrial Technology Development Organization (NEDO) entrusted to the Japan Fine Ceramics Center.

References

[1] S. Deb: J. Biomater. Appl. 14 (1999) 16-47.
[2] G. Lewis: J. Biomed. Mater. Res. 38 (1997) 155-82.
[3] S. Shinzato, M. Kobayashi, WF. Mousa, M. Kamimura, M. Neo, Y. Kitamura, T. Kokubo and T. Nakamura: J. Biomed. Mater. Res. 51 (2000) 258-72.
[4] K. Goto, M. Hashimoto, S. Fujibayashi, T. Kokubo and T. Nakamura: Bioceramics 17 (Tran Tech Publication, Switzerland 2005) p. 97-100.
[5] M. Uchida, HM. Kim, T. Kokubo, S. Fujibayashi and T. Nakamura: J. Biomed. Mater. Res. 64A (2003) 164-170.
[6] T. Kokubo, H. Kushitani, S. Sakka, T. Kitsugi and T. Yamamuro: J. Biomed. Mater. Res. 24 (1990) 721-734.